

SPHERE, a Planet Finder instrument for the VLT

Kjetil Dohlen^{*a}, Jean-Luc Beuzit^b, Markus Feldt^c, David Mouillet^b, Pascal Puget^e, Jacopo Antichi^d, Andrea Baruffolo^d, Pierre Baudoz^e, Alessandro Berton^c, Anthony Boccaletti^e, Marcel Carbillet^f, Julien Charton^b, Riccardo Claudi^d, Mark Downing^h, Christophe Fabron^a, Philippe Feautrier^b, Enrico Fedrigo^h, Thierry Fusco^g, Jean-Luc Gach^a, Raffaele Gratton^d, Norbert Hubin^h, Markus Kasper^h, Maud Langlois^a, Andy Longmore^m, Claire Moutou^a, Cyril Petit^g, Johan Pragtⁱ, Patrick Rabou^b, Gerard Rousset^e, Michel Saisse^a, Hans-Martin Schmid^j, Eric Stadler^b, Daphne Stamm^k, Massimo Turatto^d, Rens Waters^k, Francois Wildi^l

^a Laboratoire d'Astrophysique de Marseille, B.P. 8, F-13376 Marseille Cedex 12, France

^b Laboratoire d'Astrophysique de Grenoble, B.P. 53, F-38041 Grenoble Cedex 9, France

^c Max Planck Institut für Astronomie, Königstuhl 17, D-69117 Heidelberg, Germany

^d Osservatorio Astronomico di Padova, Vicolo dell'Osservatorio 5, I-35122 Padova, Italy

^e Laboratoire d'Etudes Spatiales et d'Instrumentation en Astrophysique, F-92190 Meudon, France

^f Laboratoire Universitaire d'Astrophysique de Nice, Parc Valrose, F-06108 Nice, France

^g Office National d'Etudes et de Recherches Aérospatiales, B.P. 72, F-92322 Chatillon, France

^h European Southern Observatory, Karl-Schwarzschild-Strasse 2, D-85748 Garching, Germany

ⁱ Stichting ASTRonomisch Onderzoek in Nederland, P.O. Box 2, NL-7990 AA Dwingeloo, The Netherlands

^j Institute of Astronomy, ETH Zurich, CH-8092 Zurich, Switzerland

^k Universiteit van Amsterdam, Kruislaan 403, NL-1098 SJ Amsterdam, The Netherlands

^l HEIG-VD, CH-1400 Yverdon/Observatoire de Genève, CH-1290 Sauverny, Switzerland

^m UK Astronomy Technology Centre, Royal Observatory, Edinburgh EH9 3HJ, U.K.

ABSTRACT

The Planet Finder instrument for ESO's VLT telescope, scheduled for first light in 2010, aims to detect giant extra-solar planets in the vicinity of bright stars and to characterise the objects found through spectroscopic and polarimetric observations. The observations will be done both within the Y, J, H and Ks atmospheric windows ($\sim 0.95 - 2.32\mu\text{m}$) by the aid of a dual imaging camera (IRDIS) and an integral field spectrograph (IFS), and in the visible using a fast-modulation polarization camera (ZIMPOL). The instrument employs an extreme-AO turbulence compensation system, focal plane tip-tilt correction, and interferential coronagraphs. We describe briefly the science goals of the instrument and deduce the top-level requirements. The system architecture is presented, including brief descriptions of each of the main sub-systems. Expected performance is described in terms of end-to-end simulations, and a semi-analytic performance-estimation tool for system-level sensitivity analysis is presented.

Keywords: extrasolar planets, extreme AO, coronagraph, dual imaging, polarimetry, spectral imaging

1. INTRODUCTION

After review of the two competing phase A studies^{1,2}, ESO has launched a contract for designing and building an instrument benefiting from both studies. This instrument, dedicated to Spectro-Polarimetric High-contrast Exoplanet Research (SPHERE) includes the extreme AO system (SAXO)³, the coronagraphic devices, and the differential imaging camera (IRDIS) from the LAOG et al. consortium¹ and the Integral Field Spectrograph (IFS)⁴ and the ZIMPOL dual imaging polarimeter⁵ proposed by the MPIA et al. consortium². In the following sections we present briefly the science case for SPHERE and its observational modes. We then present the global system architecture of the instrument and its main sub-systems. Finally, we present simulations showing expected performance of the instrument.

* kjetil.dohlen@oamp.fr

1.1. Science case

Following the merging of the two concepts, the science operation model has been revisited to take into account the specificities and complementarities of the different focal instruments. The prime objective of SPHERE is the discovery and study of new planets orbiting stars by direct imaging of the circumstellar environment. The challenge consists in the very large contrast of luminosity between the star and the planet (larger than ~ 12.5 magnitudes or $\sim 10^5$ flux ratio), at very small angular separations, typically inside the seeing halo. The whole design of SPHERE is therefore optimized towards high contrast performance in a limited field of view and at short distances from the central star. Both evolved and young planetary systems will be detected, respectively through their reflected light (mostly by ZIMPOL) and through the intrinsic planet emission (IRDIS+IFS modes). Both components of the near-infrared arm of SPHERE will provide complementary detection capacities and characterization potential, in terms of field of view, contrast, and spectral domain.

Within a core of ~ 100 target stars separated in several age bins, we expect to find about 10 planets with masses between a few tenths up to about $10 M_J$ with the near-infrared arm. We will be in the position to screen about 20 nearby stars for the presence of planets in their reflected light with ZIMPOL. We should stress that any detection by either of the two arms would immediately result in a characterization of the atmosphere of the extrasolar planet. A larger comprehensive survey of additional ~ 300 targets will finally lead to a statistically relevant sample of planets with masses between a few tenths up to about $10 M_J$, in the distance bin between 1 and 20 AU in a sample of more than 400 nearby stars. There is good hope that the planet orbiting ϵ Eridani will be detected and characterized by SPHERE, in which case it would be the first image and polarimetric characterization of a planet around a K2V star.

With such a prime objective, it is obvious that many other research fields will benefit from the large contrast performance of SPHERE: proto-planetary disks, brown dwarfs, evolved massive stars and marginally, solar system and extragalactic science. These domains will nicely enrich the scientific impact of the instrument. Their instrumental needs should however not be in conflict with the high-contrast requirement.

1.2. Observational modes

Three observing modes have been defined in order to draw maximum benefit of the unique instrumental capacities of SPHERE:

NIR survey. This is the main observing mode which will be used for 80% of the observing time. It combines IRDIS dual imaging in H band with imaging spectroscopy using the IFS in the Y-J bands by the aid of dichroic beam separation after the coronagraph. This configuration permits to benefit simultaneously from the optimal capacities of both dual imaging over a large field (out to $\sim 5''$ radius) and spectral imaging in the inner region (out to at least $0.7''$). In particular, it allows to reduce the number of false alarms and to confirm potential detections obtained in one channel by data from the other channel. This will be a definitive advantage in case of detections very close to the limits of the system.

NIR characterization. IRDIS used alone in its various modes will allow obtaining observations with a wider FOV in all bands from Y to short-K, either in dual imaging or in broad and narrow-band filters. This will be especially interesting in order to obtain complementary information on already detected and relatively bright targets (follow-up and/or characterization). Spectroscopic characterization at low or medium resolution will be possible in long-slit mode. Additional science cases will also benefit from these observing modes (disks, brown dwarfs, etc.). This will be a very useful capability for the ESO community at a time where NACO will most likely not be offered anymore.

Visible search and characterization. The polarimetric capacities of ZIMPOL will provide unique performance for reflected light very close to the star, down to the level required for the first direct detection in the visible of old close-in planets, even if on a relatively small number of targets. ZIMPOL also provides classical imaging in the visible, offering unique high-Strehl performance in an era when the Hubble Space Telescope (HST) will probably have been decommissioned.

2. SYSTEM ARCHITECTURE

2.1. Global overview

The proposed design of SPHERE is divided into four subsystems as illustrated in Figure 1: the Common Path Optics and the three science channels IRDIS, IFS, and ZIMPOL. The Common Path includes pupil stabilizing fore optics (tip-tilt and de-rotator) where insertable polarimetric half-wave plates are also provided, the SAXO extreme adaptive optics system with a visible wavefront sensor, and NIR coronagraphic devices in order to feed IRDIS and IFS with a highly

stable coronagraphic image in the NIR. ZIMPOL shares the visible channel with the wavefront sensor and includes its own coronagraphic system. A photon sharing scheme has been agreed between IRDIS and IFS, allowing IFS to exploit the NIR range up to the J band, leaving the H-band, judged optimal for the DBI mode, for IRDIS during the main observation program. The instrument and all its sub-systems will be mounted on an optical bench situated on one of the VLT Nasmyth platforms. The bench will be actively damped by a pneumatic servo-controlled system and equipped with a dust cover.

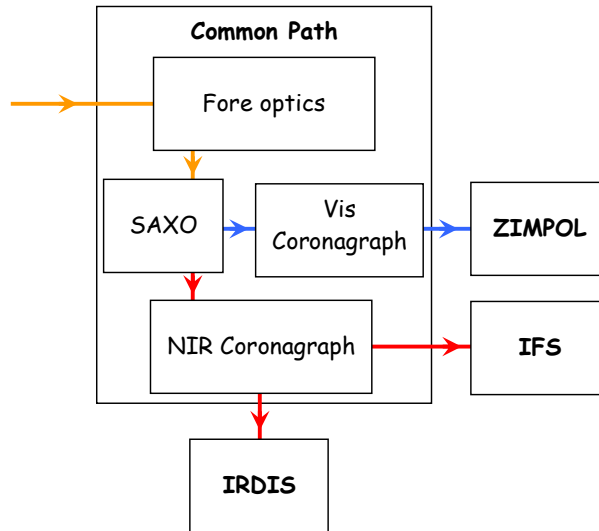


Figure 1. Global concept of the SPHERE instrument, indicating its four sub-systems: Common Path, IRDIS, IFS, and ZIMPOL. It also includes the main functionalities within the Common Path sub-system. Optical beams are indicated in red for NIR, blue for Vis and orange for common path.

2.2. Common Path optics

Figure 2 shows current design of SPHERE on the Nasmyth platform, indicating the main feature of the Common Path optics and how it feeds the other sub systems and the AO sensors. In order to optimize bench stiffness, a compact bench layout is chosen. Access to critical optics (ADCs, coronagraphs, wavefront sensor optics, ...) is ensured by a "man hole" in the bench. Other critical components are located near the edges of the table and accessed by the aid of walkways. The optical design of the Common Path is based on the use of three toroidal mirrors manufactured by spherical polishing of pre-stressed substrates. This gives perfect optical correction and provision for all the necessary pupil and image planes while benefiting from the excellent surface quality (and cost) offered by spherical polishing techniques.

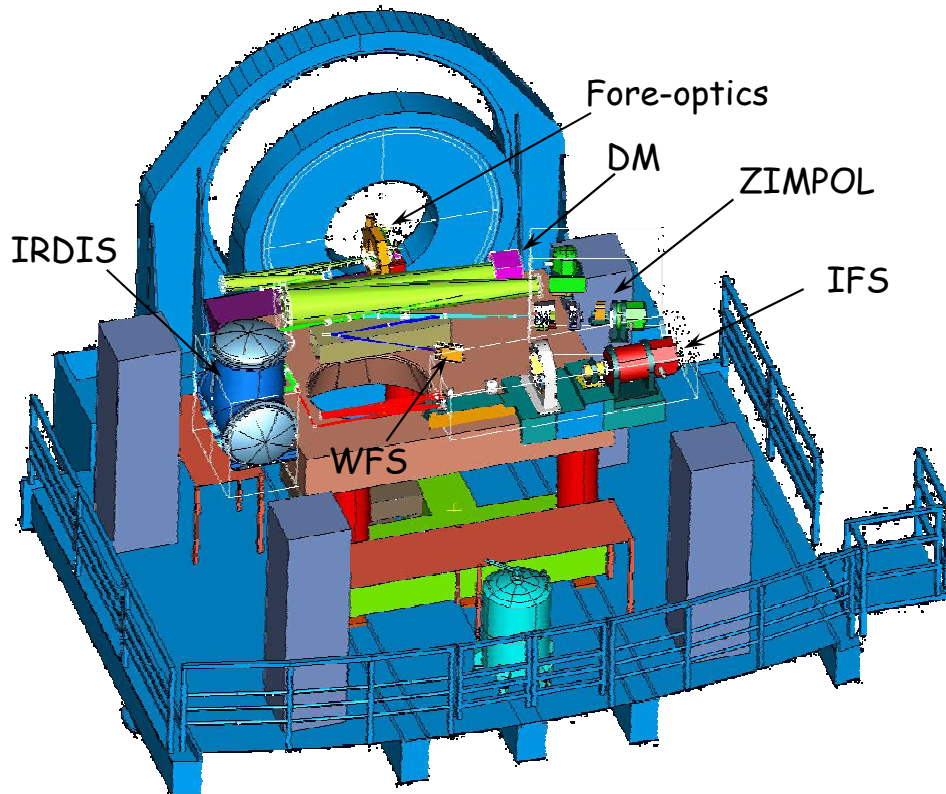


Figure 2. Implementation of SPHERE on the Nasmyth platform.

2.3. The SAXO extreme AO system

The SPHERE Adaptive optics for eXoplanet Observation, SAXO, is basically the same as the extreme AO system proposed during the Beuzit et. al. Phase A study¹. A global trade-off combining optical design, technological aspects, cost and risk issues, leads to the use of a 41x41 actuator DM of 180 mm diameter with an inter-actuator stroke $>\pm 1\mu\text{m}$ and a maximum stroke $>\pm 3.5\mu\text{m}$, and a 2-axis tip-tilt mirror (TTM) with a ± 0.5 mas resolution. The wavefront sensor is a 40x40 lenslet Shack-Hartmann sensor, with a spectral range between 0.45 and 0.95 μm equipped with a focal plane filtering device with variable size (from λ/d to $3\lambda/d$ at 0.7 μm , where d is the projected micro-lens diameter) for aliasing control. A temporal sampling frequency of 1.2 kHz is achieved using a 240x240 pixel electron multiplying CCD detector (CCD220 from EEV) with a read-out-noise $< 1e^-$ and a 1.4 excess photon noise factor. The global AO loop delay is maintained below 1 ms.

The SAXO loop structure is shown in Figure 3. Image and pupil stability are essential in high-contrast instruments. Differential image movements due to thermo-mechanical effects and ADC mechanism precision are therefore measured in real-time using an auxiliary NIR tip-tilt sensor located close to the coronagraphic focus and corrected via a differential tip-tilt mirror in the WFS arm. Likewise, pupil run-out is measured by analysis of the WFS sub-pupil intensity along the pupil edge and corrected by a pupil tip-tilt mirror close to the telescope focal plane at the entrance of the instrument. Non-common path aberrations are measured off-line using a phase diversity algorithm and compensated on-line by reference slope adjustments.

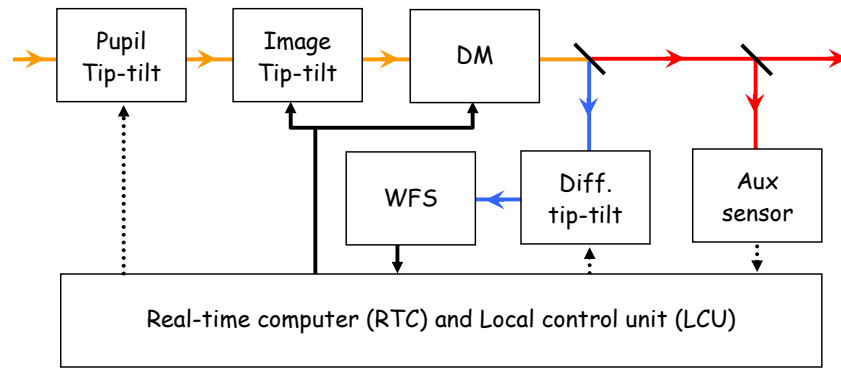


Figure 3. Conceptual drawing of the SAXO loop structure, showing broad-band beam in orange, NIR beam in red, and Vis beam in blue. Electrical signals are shown in black, solid for high-bandwidth signals ($\sim 1\text{kHz}$), and dotted for low band-width (1-10Hz). The Vis WFS and RTC generate fast signals for DM and image tip-tilt mirror (ITTM) control, as well as a slow signal for lateral pupil alignment via the pupil tip-tilt mirror (PTTM). Slow differential image motion between the Vis and NIR beams is detected using a focal plane auxiliary sensor located close to the coronagraph focus, feeding into the differential tip-tilt mirror (DTTM) located in the Vis beam.

2.4. Coronagraphs

Efficient coronagraphy is important for reaching the science goals of SPHERE. Its action is two-fold: reduce by a factor of at least 100 the intensity of the stellar peak, and eliminate the diffraction features due to the pupil edges. Stellar coronagraphy is a quickly evolving research field and it is felt to be important to leave the instrument open for future evolutions by allowing exchangeable masks both in the coronagraphic focus and in its entrance and exit pupils.

The base-line coronagraph suite will include an achromatic four-quadrant phase mask coronagraph (A4Q) based on precision mounting of four half-wave plates (HWP), and both a classical Lyot coronagraph (CLC) and an apodized Lyot coronagraph (ALC). The A4Q has recently been demonstrated in the visible, see Figure 4, where the main difficulties of precision edge-polishing and mounting of the HWPs have been addressed and excellent performance has been demonstrated⁶. Extension of these techniques to the NIR is ongoing. While the CLC option, with mask diameter of about $10\lambda/D$, is within the realm of classical manufacturing, the ALC option requires an apodizer in the coronagraph entrance pupil. Prototyping is ongoing, and a promising technology using graded metal deposition has been identified. An alternative technology based on ion implantation is also considered, but this technology gives discrete steps in the apodization profile. The effects of this are being quantified by simulations.

Other options include the classical four-quadrant phase mask⁷ which has the advantage of being very well mastered and has been intensively tested in the lab at various wavelengths (visible, near-IR, mid-IR) and on the sky with VLT/NACO⁸. More explorative options include broad-band versions⁹ of the four-quadrant phase mask based on zero-order gratings (ZOG) or its circularly symmetric version, the annular groove phase mask (AGPM), fabricated by micro-electronics process, are also being investigated. The substrate material (Si) limits both these options to the H and Ks bands.

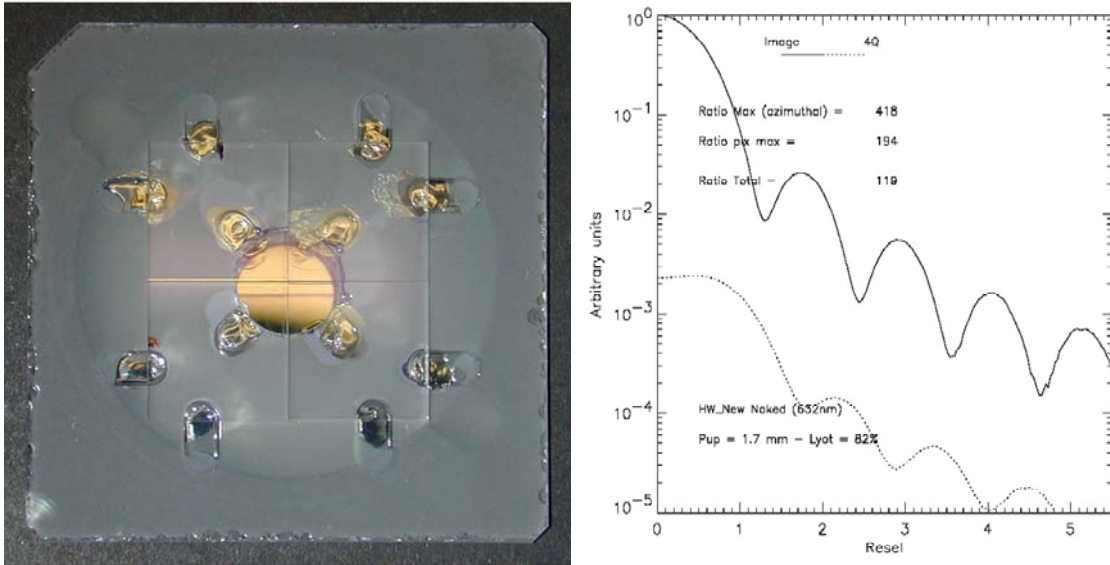


Figure 4. Prototype setup of the HWP 4QPM (left) and corresponding performance in the visible (right). The curves show radial profile without (full line) and with (dotted line) the coronagraph.

2.5. IRDIS

The Infra-Red Dual-beam Imaging and Spectroscopy (IRDIS) sub system constitutes the main science module of SPHERE. The main specifications for IRDIS include a spectral range from 950-2320 nm and an image scale of 12.25mas consistent with Nyquist sampling at 950nm. A FOV greater than 11" square is required for both direct and dual imaging, leaving a slight margin for system optimization when using two "quadrants" of a 2kx2k detector. The main mode of IRDIS is the dual imaging mode¹⁰, providing images in two neighboring spectral channels with minimized (<10nm rms) differential aberrations. Ten different filter couples are defined corresponding to different spectral features in modeled exoplanet spectra. In the direct imaging mode, 12 broad, medium and narrow-band filters are defined. In addition to direct and dual imaging, long-slit spectroscopy at resolving powers of 50 and 500 is provided, as well as a dual polarimetric imaging mode. A pupil-imaging mode for system diagnosis is also implemented.

Dual imaging separation is done using a beam-splitter combined with a mirror, producing two beams in parallel. Each beam has its own camera doublet and band-limiting filter. The main challenge is to achieve the required 10nm differential aberrations requirement, but an error budget based on high-quality classical polishing technology is found to satisfy the requirement. This option has been favored over the alternative Wollaston-based option because it eliminates spectral blurring problems, which would limit the useful FOV, and allows the use of high-quality materials with high homogeneity.

The opto-mechanical design of IRDIS is shown in Figure 5 (a). The IRDIS entrance pupil is the coronagraphic exit pupil (Lyot stop). Located in a collimated beam of diameter 10mm, it constitutes the main optical interface parameter with the common path optics. The focal ratio of the IRDIS camera lenses is 37.9, compatible with the presumed 18 μ m pitch detector arrays. Three wheels are provided within the cryogenic environment. The Lyot Stop Wheel also contains a prism and a grism for long-slit spectroscopy. It is preceded by a common filter wheel carrying narrow, medium and broad band filters for direct imaging. A second filter wheel carrying dual imaging filter pairs is located down-stream of the beam-separation unit. This mechanism also carries a pupil-imaging lens. The detector will be mounted on a two axis translation stage to allow dithering for flat-field improvement. This stage, whose development is based on CONICA heritage, will be common to both IRDIS and IFS.

The cryostat concept is shown in Figure 5 (b). In order to limit the risk in case of motor failure, the motors are mounted outside of the cold screen so as to be accessible without dismounting the bench. However, to simplify the overall design, they are kept within the cryostat. Motor replacement therefore requires breaking the thermal vacuum, but does not

require re-alignment of the instrument, limiting such interventions to below 5 days as required by ESO. Cooling power is provided by a liquid nitrogen tank with capacity for 30h autonomy. The detector will be kept at $\sim 80\text{K}$, and the optics is stabilized at a temperature below 150K to limit thermal background.

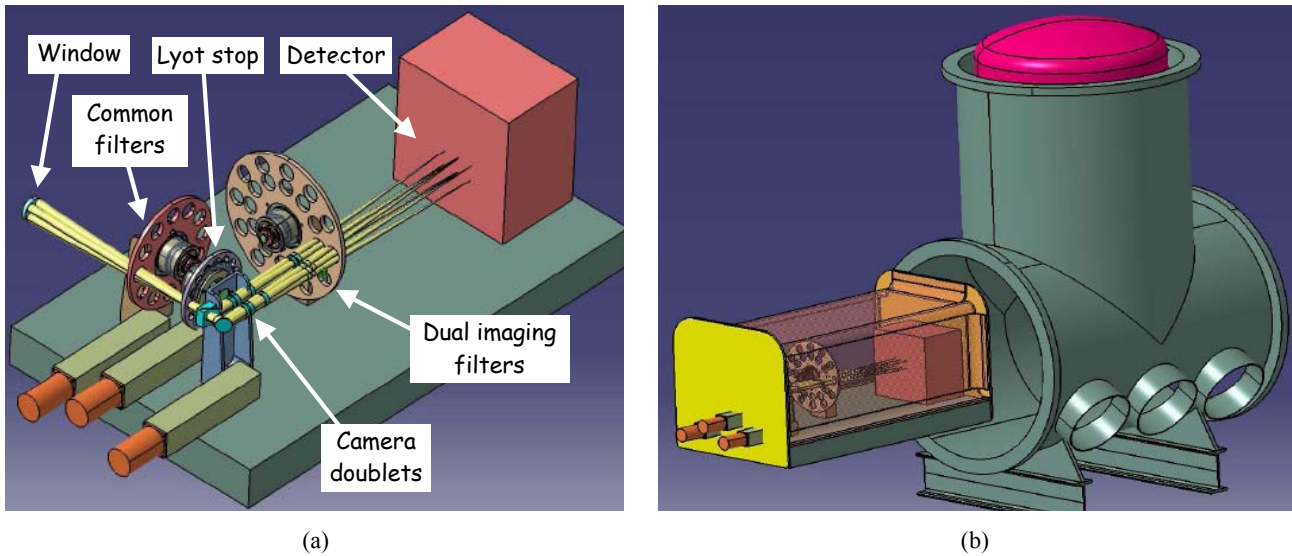


Figure 5. IRDIS opto-mechanical implementation (a) and cryostat design (b).

2.6. IFS

While an integral field spectrograph (IFS) for planet imaging is conceptually challenging, it is widely recognized as a potentially extremely useful science module for a planet searching instrument. For SPHERE we are pursuing a micro-lens based IFS concept related to the classical TIGER concept¹¹, modified for the case of high-contrast diffraction limited observations. The required $5\text{-}\sigma$ detectivity at $0.5''$ is 10^{-7} with a goal of 10^{-8} with respect to the un-occulted PSF peak, and the spectral range of the IFS is limited to the Y-J bands ($0.95\text{-}1.35\mu\text{m}$), allowing the use of a single detection channel and parallel operation of IRDIS and IFS. A resolving power per pixel of 30 is maintained, with a minimum FOV of $1.35''$ square and a strong goal of $3''$ square. Nyquist-limited spatial sampling at $0.95\mu\text{m}$ is imposed as for IRDIS. Optimized commonality between IFS and IRDIS in terms of detector and associated equipment is seen as an important system goal. The same $2\text{k}\times 2\text{k}$ detector format is therefore adopted, and it is highly likely that the long-wavelength cut off defined for IRDIS will also be acceptable for IFS.

Two different variants of the TIGER concept are considered: the Super-TIGER, and the Bigre*. In classical TIGER designs, optimized for seeing limited conditions, micro-lenses are much bigger than the diffraction pattern and provide therefore resolved images of the telescope pupil (micro-pupils) as entrance slits for the spectrograph. The spatial sampling conditions imposed on the current design imposes micro-lenses smaller than the Airy disk, and so the resulting pupil images are no longer resolved, taking themselves the form of Airy disks. As a consequence, the micro-pupils are no longer spatially limited, causing cross talk between neighboring micro-pupils, and their dimension varies with wavelength. While the Feldt et al.² Phase A study design resolved these problems by making micro-pupils much smaller than the detector pixels, this has since been shown to create problems due to speckle aliasing. Due to the chromatic evolution of the speckle scale, the stellar spectrum observed through a given micro-lens is itself speckled, with a typical speckle period which increases with separation from the star. At separations greater than $R\lambda/D$, where R is the resolving power of the spectrograph, the typical speckle period matches the resolving power, and so, for a detector-limited resolving power, speckle spectra will be aliased. This aliasing jeopardizes attempts at speckle reduction by spatio-spectral interpolation¹³ or other methods.

* The TIGER ("Traitement Intégral des Galaxies par l'Etude de leur Raies") concept got its name from sharing the focal reducer cage of PUMA¹². The Bigre concept was so named because that was the first word uttered by Georges Courtes, the inventor of the TIGER concept, after our attempt at explaining the problem of speckle aliasing and its possible resolution using a dual micro-lens array. *Bigre* is a French exclamation with a meaning similar to *Bligh-me* in English.

The Super-TIGER is a modified design in which the problems due to the pupil diffraction have been countered by making the spectral resolution diffraction limited by strongly reducing the pixel scale. This is expensive in terms of pixels and causes an important reduction in FOV. The Bigre concept minimizes speckle aliasing by making the spectrograph resolution slit-limited, as in the classical, seeing-limited TIGER concept. A second micro-lens array, whose focal length is shorter than the first one, is added after the micro-pupil mages. These secondary micro-lenses form reduced images of the first micro-lenses, i.e. of the image plane, so-called micro-images. The micro-images are spatially limited, and their size no longer depends upon wavelength. Choosing a pixel scale corresponding to half the micro-image width efficiently reduces spectral aliasing with increased pixel efficiency. This restores the FOV, but only at the cost of the increased complexity of a double micro-lens array. Figure 6 illustrates each of these basic concepts. A simulation of the resulting, dispersed image is shown in Figure 7 (right).

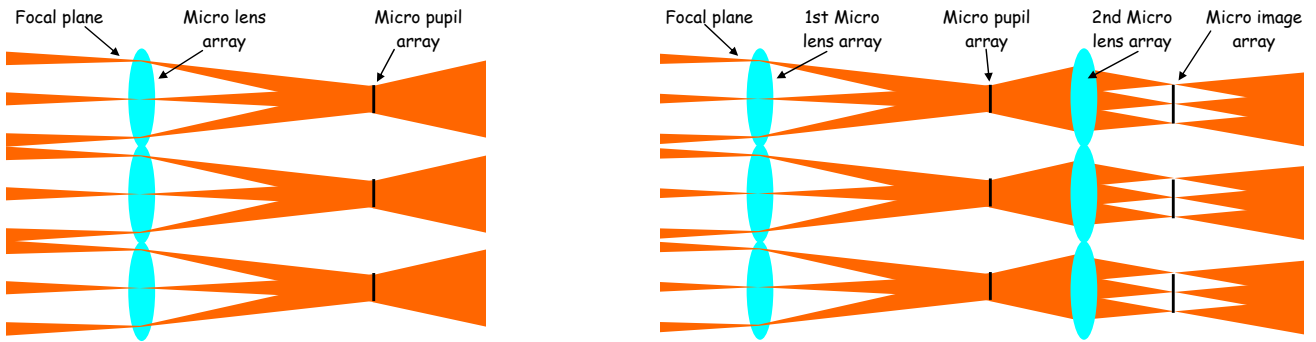


Figure 6. Optical concept of the TIGER (left) and the Bigre (right).

In addition to the micro-lens system at the entrance of the spectrograph, the opto-mechanical concept includes collimation optics, an Amici Prism providing zero beam deviation and constant resolution within the entire wavelength range, camera optics, and the detector cryostat, see Figure 7 (left). Thermal background is controlled by extending the cryostat >150mm in front of the detector, thus limiting the solid angular view of the warm environment, and by including a cold short-pass filter. As for IRDIS, a lateral detector translation mechanism will be required in order to improve flat-field precision.

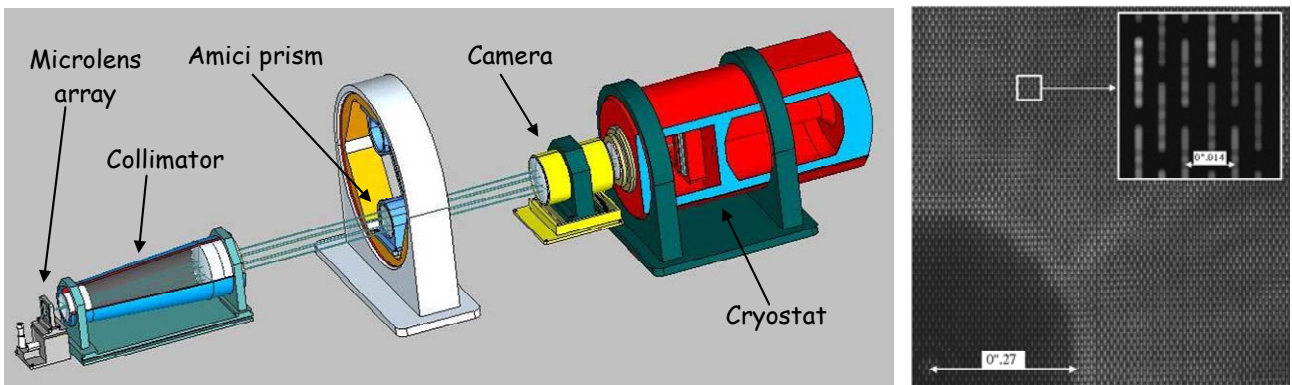


Figure 7. Opto-mechanical design of the IFS (left) and a simulated detector image (right). The zoom shows the spectrum of each individual micro-lens.

2.7. ZIMPOL

The Zurich Imaging Polarimeter (ZIMPOL) subsystem is a high-precision imaging polarimeter working in the visual range, covering at least from 600 to 900 nm. The instrument principle⁵ is based on fast modulation, using ferro-electric retarder, and demodulation of the polarization signal, using a modified CCD array, as illustrated in Figure 8 (left). Key advantages of this technique are the simultaneous detection of two perpendicular polarizations (the modulation is faster than seeing variations), and the recording of both images on the same pixel. Thanks to this approach, a polarimetric precision of 10^{-5} or even better should be achieved. The CCD will cover a Nyquist sampled field of $3'' \times 3''$ square and it is foreseen that the FOV can be moved around the bright star so that a field with a radius of $4''$ can be covered. In addition to polarimetric imaging, ZIMPOL provides the possibility for high resolution imaging in the visual range using a set of broad and narrow band filters. This capacity will be unique in the post-HST era of the years 2010.

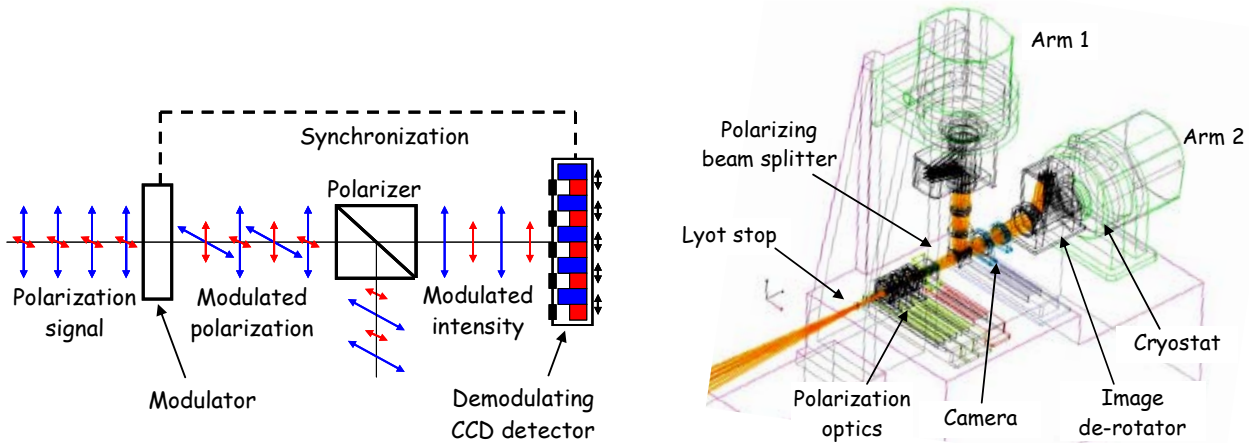


Figure 8. Basic polarimetric principle (left) and current opto-mechanical design (right) of ZIMPOL.

The opto-mechanical design of ZIMPOL from the Lyot pupil to the detectors is shown in Figure 8 (right). After the pupil follow a tilted polarization compensator plate minimizing the instrument polarization for ZIMPOL. Selectable retarder plates and polarizers allow for calibration of the remaining instrument polarization. The following modulator package consists of two components, a rotating zero order half wave plate and a ferro-electric polarization modulator. Further downstream, a polarizing beam splitter produces two beams, both of which are equipped with a filter wheel, camera lens and detector. The design shown includes image de-rotators, but these will most likely be dropped in the final design.

3. PERFORMANCE ANALYSIS

Various numerical simulation approaches have been developed by different groups during the Phase A studies of the SPHERE instrument. All these efforts are being gathered into a single instrument simulator developed on the CAOS platform¹⁴ in order to provide the technical and scientific community with a tool to predict the instrument performance. We present here the basic approach and key results of the AO/IRDIS simulator developed in Phase A, invoking a double subtraction, dual imaging approach.

Figure 9 shows the structure of the dual imaging performance simulator. Through a series of three Fourier transforms (denoted \mathcal{F} in the figure), the coronagraphic action on a perturbed wavefront and the influence of post-coronagraphic aberrations are simulated. The coronagraphic entrance wavefront is affected by time-variable residuals of the AO correction of atmospheric turbulence, as well as quasi-static instrumental aberrations. Instrumental aberrations include actual phase maps representing the VLT mirrors, and estimated phase maps of instrument optics generated using a power spectral density (PSD) with an inverse square-law radial profile, assumed to represent typical high-quality optical surfaces¹⁵. All the optics upstream of the dichroic beamsplitter is high-pass filtered with a cutoff at the AO cut-off spatial frequency ($20c$, denoting cycles per pupil diameter). All optics downstream of the dichroic is high-pass-filtered with a cut-off at $4c$, representing the expected limit of instrumental calibration based on phase-diversity techniques¹⁶. Post coronagraphic aberrations represent aberrations within the IRDIS science module. While common aberrations, as predicted by theoretical studies¹⁷, are of little influence on the speckle reduction process, differential aberrations are

extremely important. This leads to the strict differential aberrations budget imposed upon the IRDIS design. Other factors included in the simulations include image decentering on the focal plane mask, both dynamic (jitter), chromatic (ADC residual) and fixed offset, coronagraph defaults (e.g. deviation from π phase shifts in the 4QPM mask), etc. Figure 10 shows typical raw images produced by this model, without (left) and with (right) the 4QPM coronagraph.

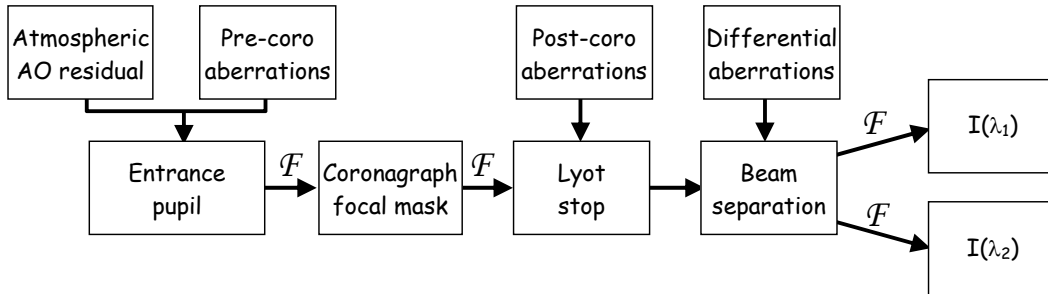


Figure 9. Basic structure of the dual imaging performance model.

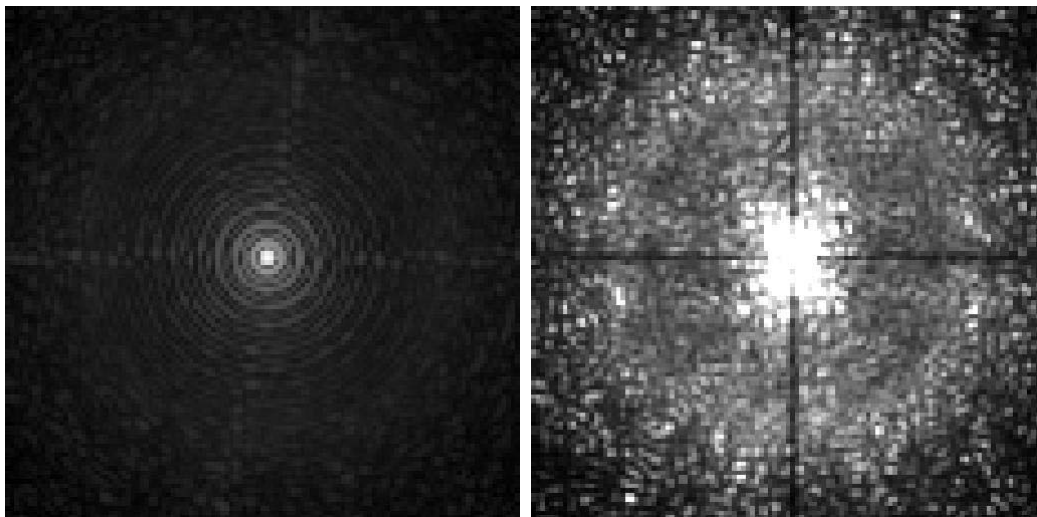


Figure 10. AO corrected bright star image without (left, non-linear with 0.1 power law) and with (right, linear with white representing $5 \cdot 10^{-5}$ of PSF maximum) a 4-quadrant phase mask coronagraph.

In the complete double difference simulation, this simulation is performed twice, once for the object star and once for a reference star, using uncorrelated atmospheric screens and introducing small differences, in particular in terms of fixed offset of the star on the coronagraph and transverse and rotational alignment error between telescope phase screens and instrument phase screens. A sensitivity analysis has confirmed the great importance of controlling these parameters to great precision (image centering < 0.5 mas, pupil shift $< 0.2\%$, pupil rotation $< 0.1^\circ$), imposing the pupil and image stabilization optics and control loops described above.

Figure 11 shows the resulting processed image after dual wavelength subtraction (left) and the complete double difference subtraction involving a reference star. The object is here a young (10 Myr) M0 star at 10 pc, with 1 MJ companions located at 0.1 to 0.4 arcsec from the star. These companions have a difference in magnitude of 12 with respect to their host star, representing a contrast of $1.3 \cdot 10^{-5}$. Through an extensive simulation of test cases involving various stellar ages and distances and a series of different sized companions at different orbital separations, we find in particular that 1 MJ planets are detectable down to angular separations of $0.2''$ for a young (10 Myr) M0 star at 40 pc, and that 10 MJ planets are detectable down to angular separations of $0.1''$ for older (1 Gyr) M0 star at 10 pc. These results are illustrated in Figure 12 showing plots of different companions intensity compared with radial variance profiles in the processed images.

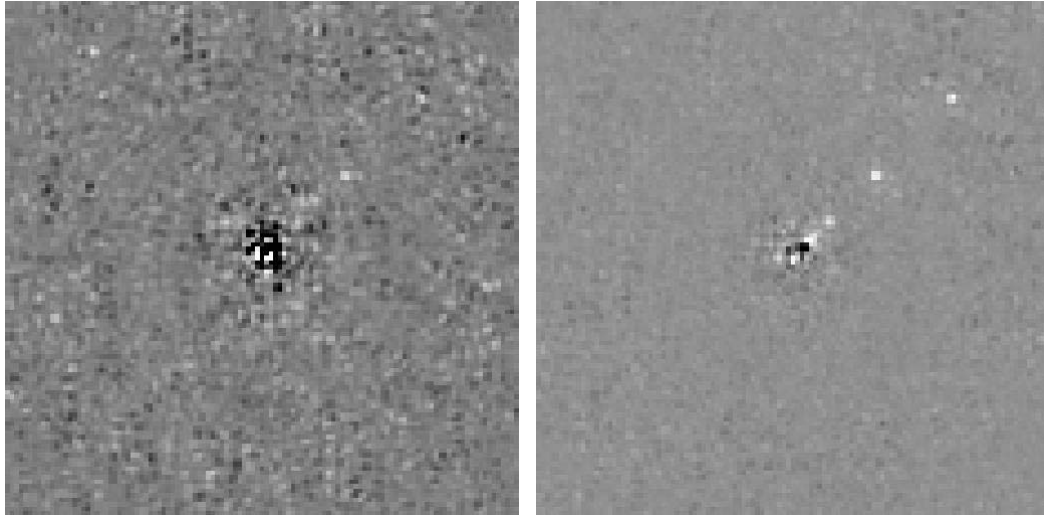


Figure 11: Residuals after simple dual band subtraction (left) and double subtraction (right). Gray scale is linear between $\pm 5 \cdot 10^{-6}$ of the non coronagraphic PSF maximum. Residual noise is subtracted down to a level much lower than companion flux.

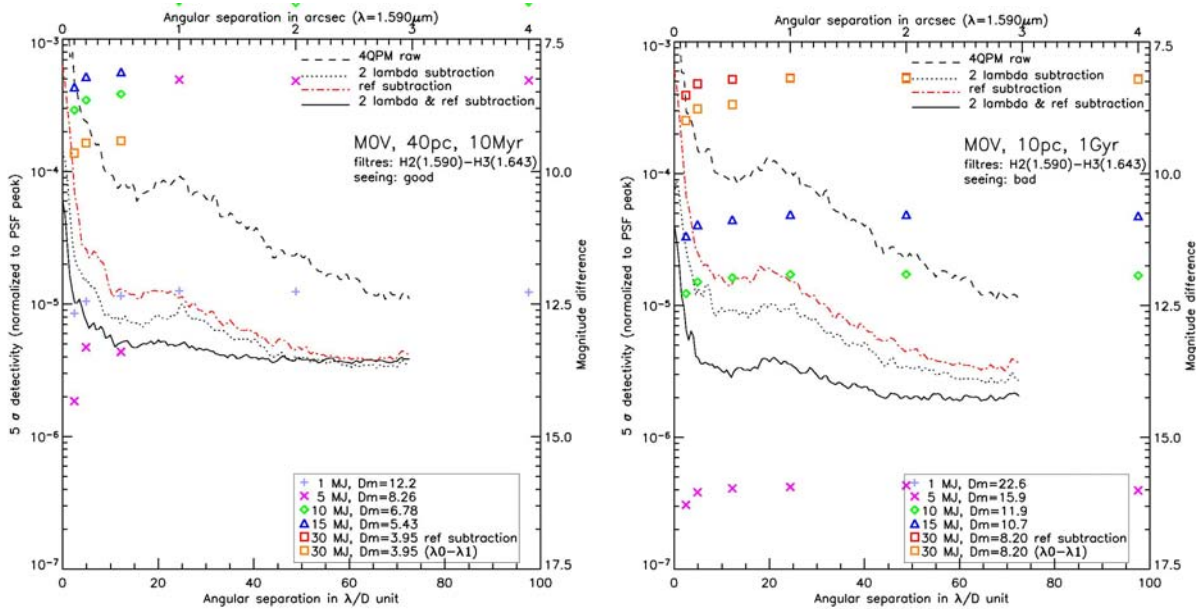


Figure 12. Companion intensities compared with radial variance profiles in the processed images. Some results of an extensive simulation of test cases involving various stellar ages and distances. 1 MJ planets are detectable down to angular separations of $0.2''$ for a young (10 Myr) M0 star at 40 pc (left). 10 MJ planets are detectable down to angular separations of $0.1''$ for older (1 Gyr) M0 star at 10 pc (right).

4. CONCLUSION

We have described SPHERE, a planet finding instrument for the ESO VLT observatory, in terms of its system design and in view of its science goals and expected performances. The conception and construction of this instrument, whose performance relies upon a state-of-the-art extreme AO system and highly performing NIR and Visible focal plane units, involves a large consortium of European institutes. The co-ordination of such a large consortium is in itself a great challenge, both in terms of resource management and interface control.

ACKNOWLEDGEMENTS

SPHERE is an instrument designed and built by a consortium of French, German, Italian, Swiss and Dutch institutes in collaboration with ESO.

REFERENCES

1. Mouillet, D.; Lagrange, A. M.; Beuzit, J.-L.; Moutou, C.; Saisse, M.; Ferrari, M.; Fusco, T.; Boccaletti, A., "High Contrast Imaging from the Ground: VLT/Planet Finder," in *Extrasolar Planets: Today and Tomorrow*, Jean-Philippe Beaulieu, Alain Lecavelier des Etangs and Caroline Terquem (eds), ASP Conf. Proc. 321, 2004, p.39.
2. M. Feldt, T. Henning, S. Hippler, M. Turatto, R. Neuhaeuser, H. M. Schmid, R. Waters "The CHEOPS project: CHAracterizing Exo-planets by Opto-infrared Polarimetry and Spectroscopy" in *Exploring the cosmic frontiers: Astrophysical instruments for the 21st century*, Proc. ESO Astrophysics Symposium (2005).
3. T. Fusco, C. Petit, J.-F. Sauvage, G. Rousset, M. Kasper, K. Dohlen, J. Charton, P. Rabou, P. Feautrier, P. Baudoz, J.-L. Beuzit, M. Downing, E. Fedrigo, D. Mouillet, P. Puget, "Design of the extreme AO system for the planet-finder instrument of the VLT," in *Advances in Adaptive Optics II*, Brent L. Ellerbroek, Domenico Bonaccini, eds, Proc. SPIE 6272 (2006).
4. R.U. Claudi, M. Turatto, J. Antichi, R. Gratton, S. Scuderi, E. Cascone, D. Mesa, S. Desidera, A. Baruffolo, A. Berton, P. Bagnara, E. Giro, P. Bruno, D. Fantine, J.-L. Beuzit, P. Puget, K. Dohlen. "The Integral Field Spectrograph of SPHERE: the Planet Finder for VLT." in: *Ground-based and Airborne Instrumentation for Astronomy*, Ian S. McLean, Masanori Iye, eds, Proc SPIE 6269 (2006)
5. D. Gisler, H.M. Schmid, C. Thalmann, H.P. Povel, J.O. Stenflo, F. Joos, M. Feldt, R. Lenzen, J. Tinbergen, R. Gratton, R. Stuik, D.M. Stam, W. Brandner, S. Hippler, M. Turatto, R. Neuhauser, C. Dominik, A. Hatzes, Th. Henning, J. Lima, A. Quirrenbach, L.B.F.M. Waters, G. Wuchterl, H. Zinnecker, "CHEOPS/ZIMPOL: a VLT instrument study for the polarimetric search of scattered light from extrasolar planets," in: "Ground-based instrumentation for astronomy", A.F.M. Moorwood & M. Iye (eds.), SPIE Conf. Vol. 5492, 463-474 (2004)
6. Mawet, D.; Riaud, P.; Baudrand, J.; Baudoz, P.; Boccaletti, A.; Dupuis, O.; Rouan, "The four-quadrant phase-mask coronagraph: white light laboratory results with an achromatic device ", *Astronomy and Astrophysics* 448, pp.801-808 (2006).
7. Rouan, D.; Riaud, P.; Boccaletti, A.; Clénet, Y.; Labeyrie, A., "The Four-Quadrant Phase-Mask Coronagraph. I. Principle," *PASP* 112, pp. 1479-1486 (2000).
8. Boccaletti, A.; Riaud, P.; Baudoz, P.; Baudrand, J.; Rouan, D.; Gratadour, D.; Lacombe, F.; Lagrange, A.-M., "The Four-Quadrant Phase Mask Coronagraph. IV. First Light at the Very Large Telescope," *PASP* 116, pp. 1061-1071 (2004).
9. Mawet, Dimitri; Riaud, Pierre, "Subwavelength gratings for phase mask coronagraphy: the 4QZOG and AGPM coronagraphs," In: *Direct Imaging of Exoplanets: Science & Techniques*, C. Aime and F. Vakili (eds). Proc. IAU 200, Cambridge (2006), pp.361-366.
10. Racine, R., Walker, G. A. H., Nadeau, D., Doyon, R., & Marois, C., "Speckle Noise and the Detection of Faint Companions," *PASP*, 111, 587 (1999).
11. Bacon, R.; Adam, G.; Baranne, A.; Courtès, G.; Dubet, D.; Dubois, J.-P.; Georgelin, Y.; Monnet, G.; Pecontal, E.; Urios, J., "The Integral Field Spectrograph TIGER," in: *Proceedings of ESO Conference on Very Large Telescopes and their Instrumentation*, Marie-Helene Ulrich (ed.), ESO 1988, p.1185.
12. Bacon, R., "The integral field spectrograph TIGER: results and prospects. In: *3D Optical Spectroscopy Methods in Astronomy*, G. Comte, M. Marcelin (eds), ASP Conf. Series 71, 1995, p. 239
13. Sparks, W. B., Ford, H. C., "Imaging spectroscopy for extrasolar planet detection," *ApJ* 578, pp. 543–564 (2002).
14. Carbillet, Marcel; Verinaud, Christophe; Guarracino, Mario; Fini, Luca; Lardiere, Olivier; Le Roux, Brice; Puglisi, Alfio T.; Femenia, Bruno; Riccardi, Armando; Anconelli, Barbara; Correia, Serge; Bertero, Mario; Boccacci, Patrizia, "CAOS: a numerical simulation tool for astronomical adaptive optics (and beyond)," In: *Advancements in Adaptive Optics*, Domenico B. Calia, Brent L. Ellerbroek, and Roberto Ragazzoni (eds). Proc. SPIE 5490, pp. 637-648 (2004).
15. Duparré, A., Ferre-Borrull, J., Gliech, S., Notni, G., Steinert, J., Bennett, J. M., "Surface characterization techniques for determining the root-mean-square roughness and power spectral densities of optical components," *Appl. Opt.* 41, 154 (2002).
16. A. Blanc, T. Fusco, M. Hartung, L. M. Mugnier et G. Rousset, "Calibration of NAOS and CONICA static aberrations. Application of the phase diversity technique," *Astron. Astrophys.*, 399 (2003), pp. 373–383.
17. Cavarroc, C.; Boccaletti, A.; Baudoz, P.; Fusco, T.; Rouan, D., "Fundamental limitations on Earth-like planet detection with extremely large telescopes," *Astron. Astrophys.* 447, (2006), pp.397-403.